NATIONAL UNIVERSITY OF SCIENCE AND TECHNOLOGY POLITEHNICA BUCHAREST

Doctoral School of Chemical Engineering and Biotechnologies

Decision no. ____ from.....

PhD THESIS
(SUMMARY)

Advanced electrochemical methods for organic pollutants oxidation

---

Author: Eng. Roberta-Geanina IRODIA

PhD Supervisor: Prof.Dr. Eng. Cristian Pîrvu

PhD Committee

President	Prof. Dr. Eng. Cristina ORBECI	from	National University of Science and Technology Politehnica Bucharest
PhD Supervisor	Prof. Dr. Eng. Cristian PÎRVU	from	National University of Science and Technology Politehnica Bucharest
Referent	CSI Nicolae SPĂTARU	from	Institute of Physical Chemistry "Ilie Murgulescu"
Referent	Conf. Dr. Eng. Elena VULPAȘU	from	Technical University of Civil Engineering of Bucharest
Referent	Conf. Dr. Eng. Mihaela MÎNDROIU	from	National University of Science and Technology Politehnica Bucharest

Bucharest
2023

Table of contents

Introduction

One of the most pressing issues today is the conservation and protection of water resources, as water is one of the most vulnerable natural resources to human activity contamination. One of the most common types of pollutants released into the environment by chemical and associated sectors is inorganic water pollutants, which can be found in products like fertilizers, medications, and refined oils. Water can be polluted by heavy metals and other inorganic pollutants when their concentrations are too high. These pollutants include trace elements, mineral acids, metals, metal compounds, inorganic salts, metals with organic compounds in the form of complexes, sulfates, and cyanides.

The presence of organic contaminants, which can be harmful or carcinogenic, in water supplies is a major cause of concern. Organic contaminants, especially those that go inland, tend to collect into rivers [1]. Detergents, colors, food processing wastes, insecticides, herbicides, petroleum hydrocarbons and lubricants, byproducts of fuel combustion, volatile organic compounds, chlorinated solvents, perchlorate (from personal care products), pharmaceutical drugs and metaabsorbents, and garbage are all examples of organic water pollutants [1, 2]. A monitoring approach can be used to control both inorganic and organic contaminants. Longer periods of contact with soil may cause chemical reactions. The rate at which these processes occur is determined by the pollutant's and soil's chemical properties [3].

Nanotechnologies have recently received a lot of attention since they have shown very high efficacy in decontaminating water and are also environmentally friendly [4].

Pollutant organic molecules are oxidized and mineralized via advanced oxidation processes, which are defined as processes that generate reactive oxidizing species. Photocatalysis is an example of cutting-edge catalytic technology that can harness the chemistry-based energy of sunlight. It can be utilized for the photocatalytic destruction of dyes, antibiotics, heavy metals, and microorganisms [5], and it is very effective and sustainable in environmental remediation. Semiconductors are utilized as photocatalysts because they conduct electricity at room temperature when exposed to light. In the last two decades, photocatalysis using TiO_2 under UV light has attracted a lot of interest as a means of cleaning up wastewater [6, 7]. TiO_2's energy band gap is 3.00-3.30 eV (depending on its crystallinity), meaning UV light irradiation is required to start its catalytic activity, and (ii)) a high rate of charge carrier recombination. Therefore, techniques are being researched to increase the efficiency of TiO_2's photocatalytic activity by extending its spectral band into the visible region by introducing defects in its own structure or by using dopants like metals, oxides, nanostructures, or even bio-inspired green materials.

KEYWORDS: electrochemistry, photoelectrocatalysis, titanium dioxide, organic pollutants, degradare, pharmaceutical compounds, nanostructures, photocatalyst

The primary goals of this thesis are to obtain and characterize new nanostructured materials based on modified TiO_2 with a lowered bandgap energy to permit irradiation with light in the visible range. In order to oxidize certain organic molecules present in water at extremely low concentrations, scientists turn to nanostructured materials. With these in mind, the thesis is organized around the pursuit of four goals:

I. For the **1st objective**, we'll conduct a study to determine the best way to produce a novel photocatalyst made from TiO_2 nanoparticles that will be deposited by dipcoating onto FTO glass. The obtained photocatalyst has good performance characteristics for mineralizing methylorange out of an aqueous solution and oxidizing organic molecules.

II. The **2nd objective** is to create a new self-doped photocatalyst out of TiO_2 nanotubes coated with TiO_2 nanofibers. These structures were functionalized, and their ability to produce photocatalytic degradation of tetracycline from an aqueous solution by photocatalysis was evaluated.

III. The **3rd objective** is to create a novel TiO_2 photocatalyst that has been doped with cobalt metal ions. Cobalt ion doping techniques (either electrochemical or plasma doping) are compared in terms of their effectiveness, as measured by the photoatalytic degradation of doxycycline in water and the resulting antibacterial action.

IV. The **4th objective** presents how to develop a new eco-friendly photocatalyst based on TiO_2 nanostructures. This hybrid photocatalysts, Polydopamine/TiO_2/Chlorophyll is environmentally friendly and stable. Degradation studies using an aqueous solution of methylorange were carried out to examine the efficacy of this novel hybrid photocatalyst.

Part I focuses on literature analysis, and **Part II** presents the originality contributions.

Literatury Studies was the focus of **the 1st part** . Four chapters detail new and relevant information about water pollution and water remediation methods.

- Chapter 1 reveals informations about water pollution issues and pollutant classification.
- Chapter 2 provides information on water depollution technologies among which advanced oxidation processes are developed.
- Chapter 3 involves literature studies regarding the photocatalytic degradation of organic compounds based on TiO_2 nanostructured semiconductor.
- Chapter 4 presents methods of characterization of photocatalysts obtained by structural and compositional analyzes and by electrochemical methods.

Part II, titled "**Original Contributions**," presents the original research that was conducted specifically to achieve the stated goals of this PhD thesis. The thesis is divided into five sections, the first four of which detail the experiments performed and published in the academic literature, and the fifth and final section presenting the conclusions of thesis's overarching findings.

- Chapter 5 "**TITANIUM DIOXIDE THIN FILMS PRODUCED ON FTO SUBSTRATE THROUGH THE SOL-GEL PROCESS**" presents a study of optimizations for obtaining TiO_2 films in which the optimal number of coating layers by immersion and the effect of a dispersant added to the precursor solution are presented. These surfaces show efficient photocatalytic properties.
- Chapter 6 "**PHOTOCATALYTIC DEGRADATION OF TETRACYCLINE WITH TiO_2 NANOTUBES COATED WITH TiO_2 NANOFIBERS**" demonstrates that the deposition method of TiO_2 nanofibers synthesized by the electrospinning method on anodized TiO_2

nanotubes has a great influence on the surface properties influencing the optical and photocatalytic properties.

- Chapter 7 "**DEVELOPMENT OF A TIO_2-COBALT CATALYST**" involves obtaining a new photo-electro-catalyst designed for the degradation of DOX from wastewater. Moreover, this study aims to emphasize the dual functionality of the obtained photocatalyst.
- Chapter 8 "**OBTAINING A GREEN, STABLE AND EFFICIENT PHOTOCATALYST BASED ON POLYDOPAMINE/TiO_2/CHLOROPHYLL**" involves obtaining a nanostructured TiO_2 surface, modified with sustainable organic compounds such as Polydopamine (PD) bio-inspired from sea shells and/or Chlorophyll (Chl) green material extracted from spirulina to obtain a hybrid photocatalyst. These TiO_2 heterostructures have made substantial contributions to improve the photocatalytic degradation of contaminants.
- the doctoral thesis concludes with the Chapter: "**FINAL CONCLUSIONS**" and "**FUTURE RESEARCH DIRECTIONS**", this chapter summarizing the main findings from the originality part of the thesis, as well as future research perspectives.

CHAPTER 5.

TITANIUM DIOXIDE THIN FILMS PRODUCED ON FTO SUBSTRATE BY THE SOL-GEL PROCESS

This study represents an optimization study with applicability in electrocatalytic photodegradation and further presents the optimal number of dip coating layers and the effect of polyethylene glycol (PEG) dispersant added to the sol-gel precursor solution on the optical properties, the electrochemical effect, and on the properties of the titanium dioxide thin films obtained on the FTO substrate.

5.1 MATERIALS AND METHODS

5.1.1 Solutions and materials used for the photocatalyst obtaining

In this subchapter, the materials and substances that were used for the experimental studies were presented.

5.1.2 Preparation of TiO_2 Thin Films on FTO Substrate by Dip-Coating Method

The sol–gel precursor solution (solution 1) was created by mixing together 8 mL Ti(OBu)4, (as alkoxide), 80 mL ethanol (as solvent), 8 mL acetylacetone (as catalyst), 8 mL CH_3COOH (as pH adjuster, to 6) and 8 mL of water. A clear solution was obtained after 3 h of stirring the mixture at 50°C, which was further aged for 24 h at room tempera-ture. The FTO substrates were cleaned with ethanol, acetone, and distilled water for ten minutes each, then dried in air.

The resulting film was dried in an oven at 200 °C for 10 min after each deposition cycle for the organic solvent evaporation. To obtain films with different thicknesses, the deposition procedure was repeated 2, 4, 6 and 8 times. The names of the samples obtained by this method are listed as “Pnumber layer”. Then, the obtained films were investigated to determine the ideal number of layers needed to generate a TiO_2 film with a lower band gap energy and higher Urbach energy.

After determining the optimal number of TiO_2 layers, we investigated how the presence of a dispersant in the precursor solution influences the nanomorphology of the mate-rial, electrochemical and optical properties of the resulting TiO_2 film. In order to accomplish this, a second solution identified as Solution 2 was made by continuously stirring solution 1 for a period of two hours, until a specific amount of PEG was dissolved. PEG promotes nanopore formation and reduces TiO_2 nanoparticle aggregation. The names of the samples that were obtained using this method are identified as follows: “Pnumber layer_PEG”.

5.1.3 Characterization Methods

In this sub-chapter, the investigation methods used, such as optical properties, physico-chemical characterization and electrochemical testing, were presented

5.2 RESULTS AND DISCUSSIONS

5.2.1 Determining the optimum number of Dip-Coatings required to deposit the TiO_2 Film on the FTO Substrate

According to the AFM image in Fig. 5.2a, the TiO_2 film produced by two cycles of dip-coating exhibited both tubular and palletized morphologies. The tube dimensions are around 3–5 µm in length and 0.65 µm in width and the pallet constructions have side lengths of 1.4 µm and 0.7 µm. The structures' heights range from 100 to 200 nm.

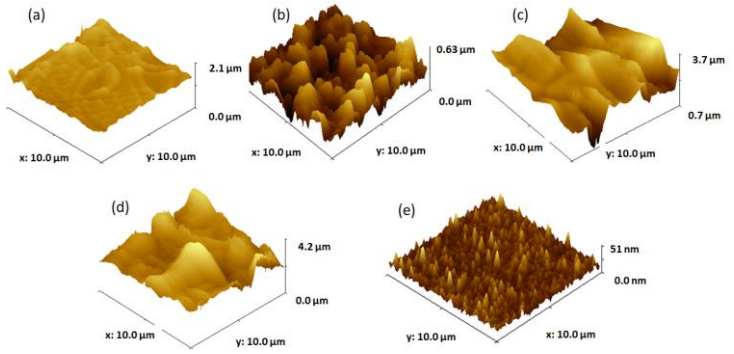

Fig. 5.2 AFM images of TiO_2 films obtained from solution 1 by (a) two dip-coating cycles, (b) four dip-coating cycles, (c) six dip-coating cycles, (d) eight dip-coating cycles, and (e) FTO substrate.

The topography of the formed film by four dip-coating cycles on the FTO substrate (Figure 5.2b) shows that the FTO substrate is completely covered by intricate TiO_2 structures. The TiO_2 structures are irregular clusters of around 1–2 µm in length and 200–400 nm in height. The TiO_2 films formed by six and eight cycles of dip-coating deposition on FTO (Figure 5.2c,d) completely cover the substrate with irregular TiO_2 dome-like structures of 3 µm in width and heights ranging from 400 to 700 nm. The topography of the FTO sub-strate on which the TiO_2 films were deposited by dip-coating (Figure 5.2e) reveals that the FTO (fluorine-doped tin oxide) particles are granular in appearance and uniformly cover the glass substrate, with grain diameters ranging from 10 to 50 nm and heights from 10 to 25 nm.

The optical transmittance spectra of TiO_2 thin films deposited from Solution 1 on the FTO substrate in the wavelength range of 300–800 nm are shown in Figure 3a as a function of the number of dip-coating layers.

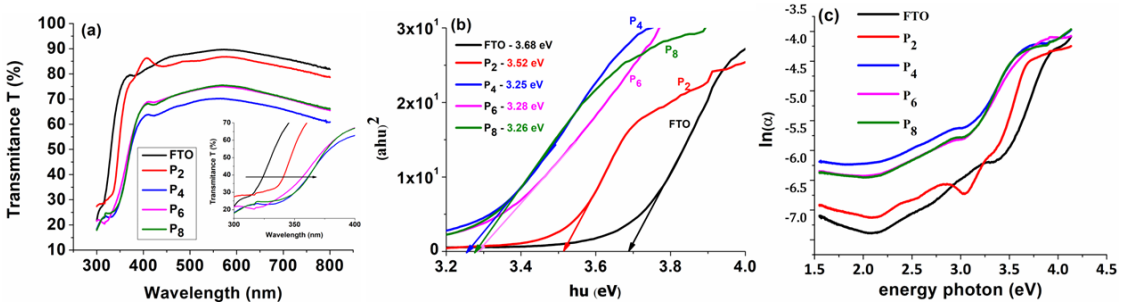

Fig. 5.3 (a) Optical transmittance; (b) plot of (αhν)2 versus hν; and (c) ln(α) versus photon energy plot for TiO_2 thin films deposited on an FTO substrate from solution 1, using different number of dip-coating layers.

The band gap value decreases with the increasing number of dip-coating deposition cycles, remaining nearly constant after four deposition cycles, at around 3.26 eV ± 0.2 eV.

Defects in the film lattice in the optical band gap region are represented by the Urbach energy (band tail width), (E_u), in Figure 5.3c).

Table 5.2 displays the calculated band gap energy and Urbach energy of TiO_2 thin films after two, four, six and eight dip coating cycles.

Table 5.2. Band gap and Urbach energies for TiO_2 thin films deposited on FTO substrate using sol–gel dip-coating at varying cycle numbers.

Number of Layers	Band Gap Energy, E_g (eV)	Urbach Energy, E_u (eV)
2	3.52 ± 0.018	0.3104 ± 0.005
4	3.25 ± 0.013	0.6459 ± 0.012
6	3.28 ± 0.017	0.6142 ± 0.011
8	3.26 ± 0.009	0.61337 ± 0.013
FTO	3.68 ± 0.018	0.2787 ± 0.013

The band gap energy (E_g) is found to decrease from 3.52 eV to 3.25 eV as the number of layers increases, while the Urbach energy increases from 310 meV to 646 meV. Based on the AFM results, it can be observed that, due to the appearance of many microcracks in P6 and P8, the band gap slowly increased and Urbach energy decreased, compared with sample P4, which presented a uniform compact film.

Furthermore, cyclic voltammetry (CV) was performed to examine the relationship be-tween the number of layers and the adherence of the obtained TiO_2 layers on the FTO sub-strate (Figure 5.4). Thus, 100 CV cycles were recorded for all samples, to determine the elec-trochemical stability of the films on the FTO substrate. Results are illustrated in Figure 5.4. As the number of CV cycles grew, the corresponding constant current values for P4 indicated (Figure 5.4b) a strong bond on the substrate and good electrochemical stability.

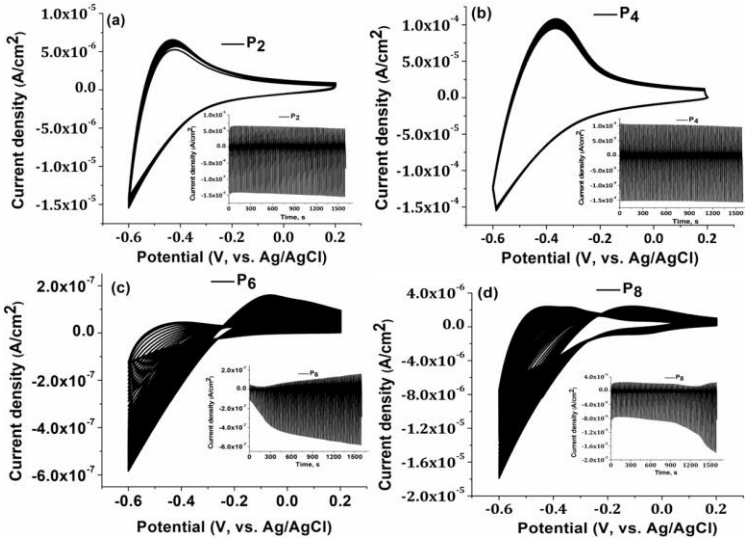

Fig. 5.4 Cyclic Voltammetry for (a) P2; (b) P4; (c) P6; (d) P8 between −0.6 V and 0.2 V vs. Ag/AgCl at 50 mV s^{-1}, 100 cycles, in 0.5 M H_2SO_4 aqueous solution.

The greater the film's electrochemical stability, the better it adheres to the substrate. Samples of both types, P2 and P4, are stable, with P4 showing a more capacitive behavior. In the samples of P6 and P8, the results changed substantially after almost 20 CV cycles. Micro-cracks in samples P6 and P8 cause an unstable CV signal and a higher optical trans-mittance compared to sample P4, as shown by a correlation between the CV test results, the AFM results, and the optical properties.

Based on the current experimental results, it has been concluded that four-cycle dip-coating is the ideal approach for depositing TiO_2 multilayers onto FTO substrates, be-cause it has the best optical properties and because it presents electrochemical stability.

5.2.2. Evaluating the impact of the PEG presence in the Sol–Gel precursor solution on the properties of TiO_2 films

5.2.2.1 Surface Characterization

All data presented represent the results obtained for samples obtained after four cycles of dip coating in solution 1 and in solution 2.

The SEM image (Figure 5.5 a) obtained for the surface of the P4 film indicates a compact and uniform TiO_2 thin layer with a homogeneous distribution of nanoparticles with an average size of around 23 nm (±2.93), which covers the whole FTO surface.

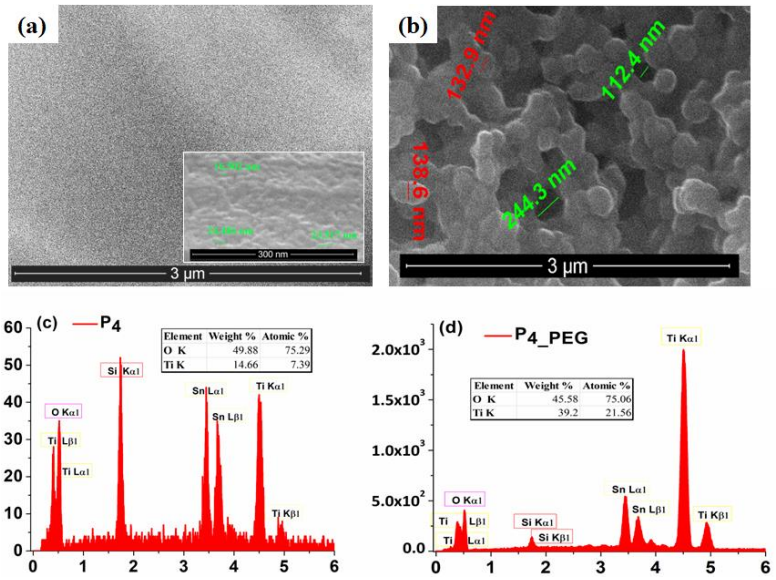

Fig. 5.5 SEM images of (a) P4 and (b) P4_PEG. EDX analysis of (c) P4 and (d) P4_PEG.

Conversely, the morphology of the P4_PEG films (Fig. 5.5 b) shows the FTO substrate covered by a continuous TiO_2 film with a homogeneous distribution of nanoparticles with an average size of around 100 nm (±6.85). As in the literature, the addition of PEG in the coating solution promoted the growth of a nanostructured film and enhanced the production of nanoparticles.

These SEM results demonstrate that the dispersant can modify the size and shape of TiO_2 nanoparticles deposited on the FTO substrate by the dip-coating method.

To confirm the presence of both Ti and O in the films obtained from both solutions, the EDX spectra (Figure 5.5 c-d) was performed and recorded. Oxygen is present in nearly equal amounts in both films, while Ti is more abundant in the P4_PEG film.

The crystalline phase and grain size of the films dip-coated on FTO were investigated using X-ray diffraction patterns (Figure 5.6).

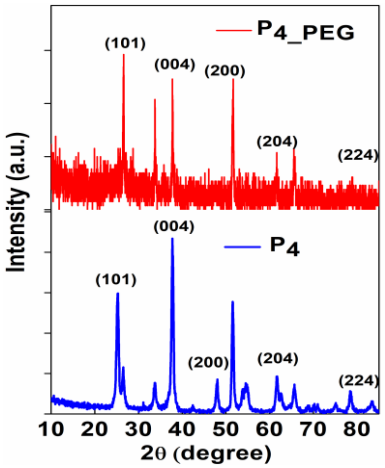

Fig. 5.6 The X-ray diffraction (XRD) patterns of P4 and P4_PEG thin films dip-coated on FTO substrate.

PEG in solution 2 increases the crystallite size while decreasing the strain, and it is expected to influence optical properties in relation to the band gap's low energy.

Surface free energy, which is a result of film surface defects, is important for the pseudo-capacitive processes that occur in many applications. The results of this study indicate that the TiO_2 films' surface free energy varies with the addi-tion of the dispersant. The Owens–Wendt–Rabel–Kaelble (OWRK) model was successfully applied to calculate the surface free energy. In terms of contact angles, the lower the surface energy, the greater the contact angles.

Table 5.4. Surface energy of TiO_2 film as a function of dispersants added in sol–gel solution.

Samples	Contact Angle, (°)			Surface Energy, (mJ m^2)
	DI Water	EG	DMSO	
P_4	26 ± 0.67	17 ± 0.24	29 ± 0.14	67
P_{4_PEG}	16 ± 0.21	5 ± 0.84	3 ± 0.60	71

5.2.2.2 Electrochemical Characterization

The electrochemical behavior of TiO_2 films in 0.5 M H_2SO_4 solution was investigated during the cycling of applied potentials ranging from −0.6 to +0.2 V at different scan rates of 25, 50, 100, 150, 200, and 300 mV s^{-1}. Both obtained films exhibited an oxidation peak near to the Fermi level of anatase TiO_2 at −0.5 V.

To investigate the charge-transfer kinetics and mass transport behavior of the films developed on the FTO substrate, electrochemical impedance spectroscopy (EIS) analysis was performed. The EIS measurements were made in a frequency range of 10 mHz to 100 kHz. Figure 5.9 shows the Nyquist plots of the P4 and P4_PEG thin films measured at free potential voltage in 0.5 M H_2SO_4 solution.

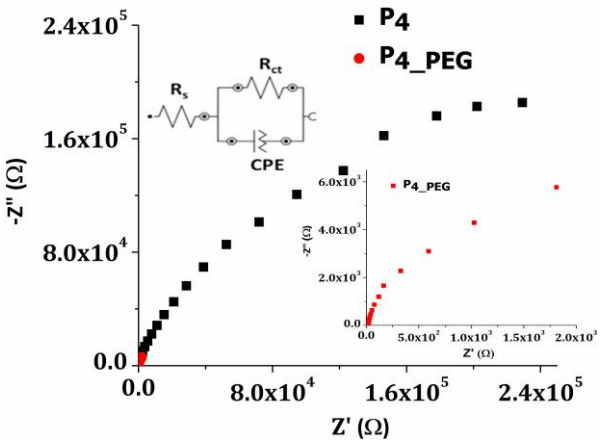

Fig. 5.9 Nyquist plots for P4 and P4_PEG films.

The Mott-Schottky (MS) equation was used for further analysis of the impedance data. Each P4 and P4_PEG film displayed a positive slope on the Mott–Schottky graphs, as is typical for n-type semiconductors, (Fig. 5.10).

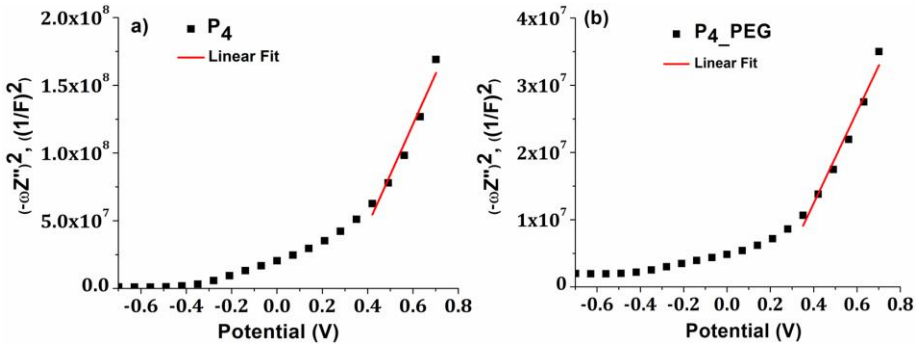

Fig. 5.10 Mott–Schotky (M-S) plots for (a) P4 and (b) P4_PEG films.

Efb is typically regarded as the conduction band potential (CB) for n-type semicon-ductors. The calculated value of Efb vs. NHE (normal hydrogen electrode) for P4 and P4_PEG is 0.055 eV and −0.019 eV, respectively. These results imply a slower recombination rate for film formed in the presence of a dispersant, which agrees with the reduction in charge-transfer resistance measured by EIS. The negative shift in the flat-band potential for P4_PEG suggests that the energy barrier for interfacial electron transport is reduced, resulting in a lower charge-transfer resistance. Moreover, the doping level (N_D) for P4 and P4_PEG are 6.5 × 1019 cm^{-3} and 2.01 × 1020 cm^{-3}, respectively, correlating with the variation in Ur-bach energy values. We may conclude that adding PEG to the sol–gel precursor solution induces a shift in the flat band potential of TiO_2 to negative values, indicating improved catalytic capabilities and a higher doping level.

5.2.2.3 Optical Properties—Bandgap and Urbach Energies

The band gap (Eg) values for P4 were reduced from 3.25 eV to 3.12 eV for P4_PEG, indicating that the films are more conductive (Figure 5.11). In addition, for thin films made with a dispersant, the Urbach energy increased from 0.645 eV to 0.709 eV.

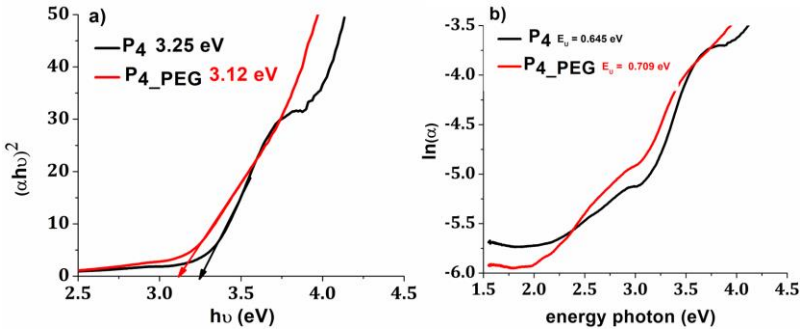

Fig. 5.11 (**a**) plot of $(\alpha h\nu)^2$ versus hν; and (**b**)plot of ln(α) versus photon energy.

The structure diagrams for the obtained films based on the measured flat band potential and band gap from the UV–VIS data are shown in Fig. 5.12. Based on the measured CB and Eg, the valence band (VB) energy of the films deposited on the FTO was computed. Based on these findings, the P4_PEG/FTO electrode can be employed in a variety of ap-plications, including smart windows and photocatalysts for solar cells or water splitting, where pseudo-capacitive behavior is desired.

5.2.3 Photocatalytic degradation

It was recorded an UV-Vis spectra of the MO solution after photodegradation, experiment performed at pH 5. In the presence of the P4_PEG catalyst, the MO solution shows a spectrum with the maximum observed at 510 nm. It is well known that the color of dyes such as methyl orange is characterized by (–N=N–) bonds and their associated chromophores and auxochromes. Visible absorbances at 510 nm decreased with irradiation time up to 180 minutes.

Therefore, UV-Vis degradation experiments of aqueous methyl orange solutions in the presence of P4_PEG follow first-order reaction kinetics. The value of the reaction speed k, can be obtained directly from the linearity of the first order equation. Under the experimental conditions, taking into account the concentration of methyl orange present in the solution after adsorption in the dark, it can be assumed that most of the photons reaching the solution are absorbed by TiO_2 (P4_PEG). They signify the presence of a heterogeneous photocatalytic process and the experimental results can be explained in terms of two elementary mechanisms: (i) oxidation of the dye through successive attacks by the hydroxyl radical ($HO^{\cdot}$); (ii) direct reaction of the dye with photogenerated holes.

In conclusion, the MO concentration in the solution decreases with increasing light exposure time in the presence of the P4_PEG catalytic surface, showing that MO photodegradation reached 56% efficiency.

CHAPTER 6

PHOTOCATALYTIC DEGRADATION OF TETRACYCLINE WITH TiO_2 NANOTUBES COATED WITH TiO_2 NANOFIBERS

In this work it was demonstrated that the deposition method of TiO_2 nanofibers synthesized by the electrospinning method on anodized TiO_2 nanotubes has a great influence on the surface properties influencing the optical and photocatalytic properties. The photocatalytic degradation of TC under UV-Vis irradiation in aqueous solution was examined in this study, using TiO_2 nanotubes coated TiO_2 nanofibers photocatalyst.

6.1 MATERIALS AND METHODS

6.1.1 Initial pretreatment

6.1.1.1 Electrochemical anodization process

TiO_2 nanotubes (TiO_2-NTs) were prepared as found in literature by anodization using the pretreated Ti plate as working electrode with the size of 2,5 cm^2 and a graphite as a counter electrod, keeping the working distance between those 2 electrods for 2 cm. The electrolyte solution contains a mixture of 0,4 wt. % NH_4F, 2wt. % H_2O and ethylenglycol (EG).

The anodization was made using a laboratory DC power suply at 30 V during 3 h and after this process took place, anealling is performed at 450^{o}C for 2 h in order to obtain a better cristalinity phase of TiO_2.

6.1.1.2 Electrospinning process

In order to obtain TiO_2 nanofibers (TiO_2-NFs), it is necessary to prepare a precursor consisting of a polyvinylpyrrolidone PVP-carrier polymer, an alkoxide precursor such as Titanium Butoxide (IV) and a mixture in a molar ratio 1:1 N,N dimethylformamide DMF and isopropanol, following to add a known amount of glacial acetic acid. The sample was magnetically stired for about 4-5 h and the solution is used therefor as a precursor for electrospinning.

6.1.2 Photocatalytic test

In order to perform photocatalytic testing, sample is placed into 10 mL of Tetracycline hydrocloride aqueous solution (TC), which has a initial concentration of 5 mg/L. Photocatalytic test was performed during 240 minutes under stirring and visibile light irradiation. Samples were taken every 10 minutes and analyzed using a spectrophotometer to measure the concentration of TC degradation in time.

6.2 RESULTS AND DISSCUSIONS

6.2.1 Deposition process

A. In order to obtain TiO_2 nanotubes coated with TiO_2 nanofibers, a previously anodized titanium plate is taken and supposed to electrospinning. By fixing the plate on the collector plate, nanofibers are electrostatically attracted to the surface, thus creating adhesion between the active surface of TiO_2 Nanotubes and the obtained TiO_2 nanofibers. The samples are subjected to calcination at 450^{o}C for 4 hours in order to remove the carrier polymer. A new photocatalyst TiO_2-NT/NF ES (TiO_2-Nanotubes/Nanofibers coated by electrospinning) was obtained.

B. TiO_2-NFs were detached from the surface by ultrasonication in distilled water making a nanofibers suspension which is introduced in a spray in order to attach NFs layer on the TiO_2-NTs

created before by anodization method. After spraying took place, the samples were introduced into the oven at 100ºC for half an hour, and so on this nanostructures TiO_2-NT/NF S (TiO_2-Nanotubes/Nanofibers coated by suspension) will improve the photocatalytic degradation efficiency.

6.2.2 Surface and optical measurements

6.2.2.1 SEM Characterization

TiO_2-NT/NF ES

The distribution of TiO_2NTs and TiO_2NFs on the surface is uniform and the nanofibers appear to be like a cap for the nanotubes, slightly covering the nanotubes.

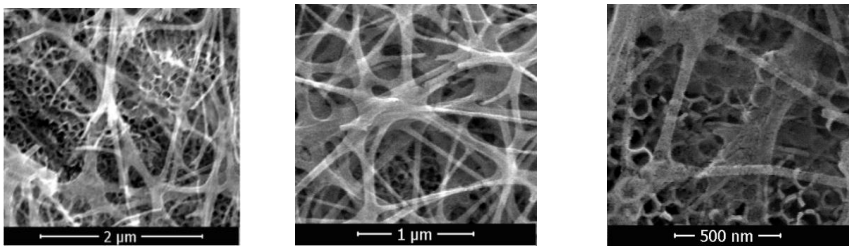

Fig. 6.3 SEM images at different magnifications of TiO_2-NT/NF ES

TiO_2-NT/NF S

As can be seen from this SEM figure below TiO_2-NTs were uniformly distributed on the entire sample surface of a Ti plate over which TiO_2-NFs have been sprayed. The surface consist of a well-organized and homogeneous arrangement of TiO_2-NTs with an average diameter of 80 nm.

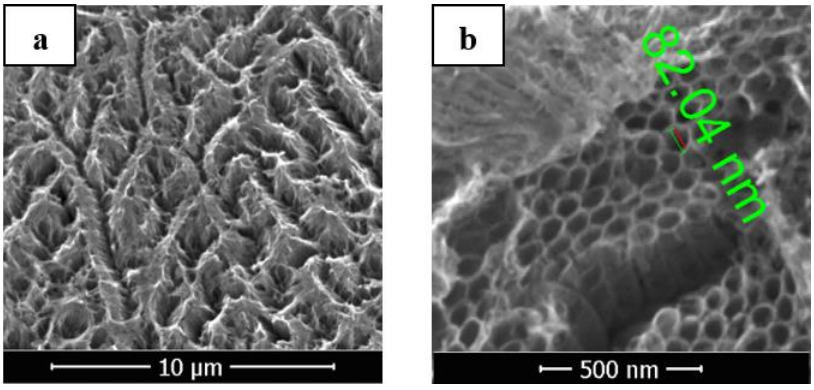

Fig. 6.4 Top view of SEM images of a) TiO_2-NTs coated with TiO_2-NFs seen at different magnifications b) TiO_2-NTs coated TiO_2-NFs

6.2.2.2 Optical measurements. Band-gap energy

Here, we report the identification of TiO_2 anatase nanosurface with a decreased bandgap that improve activation of the solar spectrum region [8].

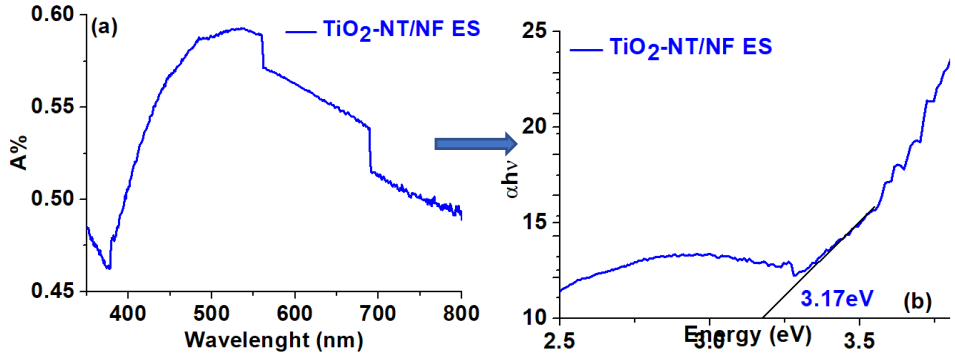

Fig. 6.8 a) UV-Vis spectrum of TiO_2-NT/NF ES b) Tauc plot diagram and band gap energy of TiO_2-NT/NF ES

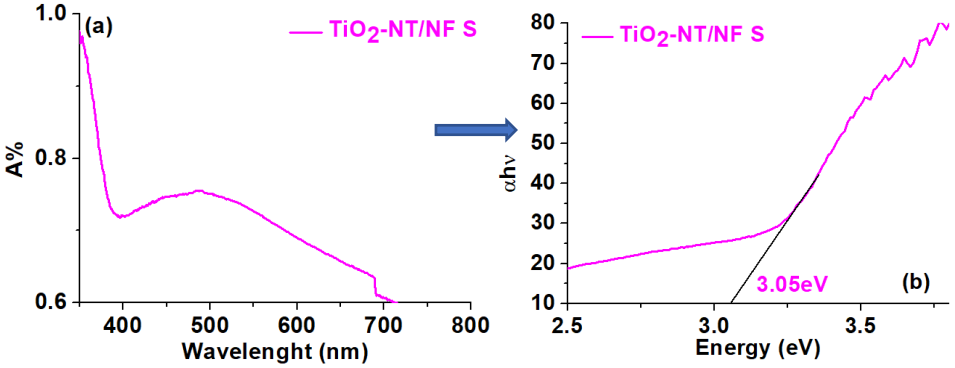

Fig. 6.9 a) Recorded UV-Vis spectrum of TiO_2-NT/NF S b) Tauc plot and band gap energy of TiO_2-NT/NF S

From Fig. 6.8 and Fig. 6.9 comparing the two samples, a decreased band gap energy is well observed this is clearly due to methods of depositing TiO_2 nanofibers on the previously anodized sub-shelf.

6.2.3 Evolution of photocatalytic degradation

An UV-Vis equipment operating at different wavelenghts was used to determine the concentration of TC at 360 nm. For the measurement of the concentration and amount of TC in the solution supposed to photocatalytic degradation, a standard calibration curve is needed and was performed using TC hydrocloride solution at several dilutions.

Further, the photodegradation of TC over TiO_2-NT/NF ES and TiO_2-NT/NF S was assessed under UV-Vis light irradiation. These studies were carried out three times each. The amount of TC in solution is more decreasing with increasing light exposure time in the presence of TiO_2-NT/NF S (Fig. 6.11 b)) catalytic surface, showing that photodegradation of TC reached 80% efficiency. These results show that the catalytic surface TiO_2-NT/NF S is more efficient for the proposed application.

With the estimation of the final concentration after time t, the kinetics of the photodegradation of TC by TiO_2-NT/NF S photocatalyst under various conditions were studied. A graph based on first-order kinetics was utilized and constructed to adapt the reaction to the appropriate kinetics. Figure 6.12 b) shows a graph of the first-order kinetics of the reaction between TC solution and TiO_2-NT/NF S photocatalyst.

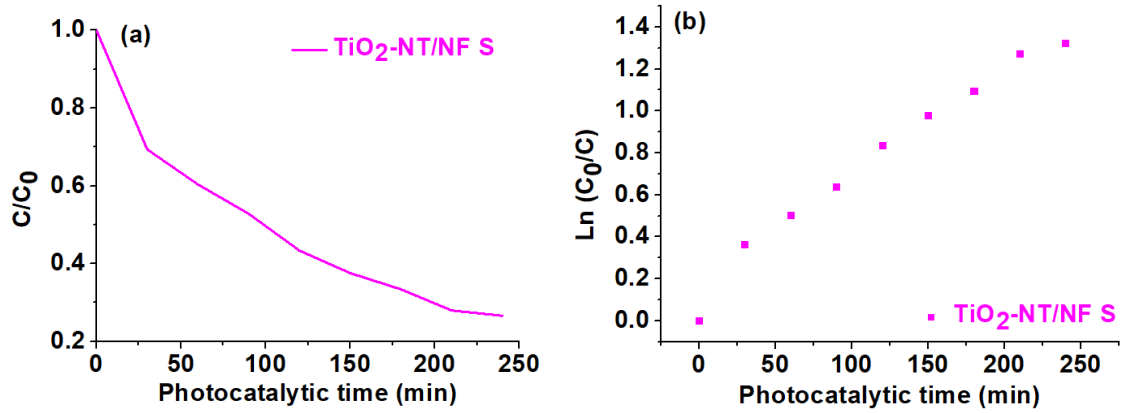

Fig. 6.12 a) TC photodegradation efficiency over TiO_2-NT/NF b) First-order kinetics graph of photodegradation of TC with TiO_2-NT/NF S photocatalyst.

Using a pseudo first order kinetic equation, it have been shown the behavior of catalyst when exposed to light, so according to Langmuir-Hinshelwood equation, the apparent first-order rate constant, k, was calculated [9].

Figure 6.12 also provides the appropriate kinetic constants and regression coefficients for the photocatalysis of TC by TiO_2. The rate constants of photodegradation of TC with TiO_2-NT/NF S is $5.3.10^{-3}$ min^{-1} , having a correlation coefficient of $R^2 = 0.9870$. The applicability in photocatalytic degradation of the TiO2-NT/NFS catalyst was demonstrated in the degradation of TC hydrochloride solution during 240 min of light irradiation. It should be noted that the degradation of TC has occurred almost completely.

CHAPTER 7

DEVELOPMENT OF A TiO_2-COBALT CATALYST

In this study, a new photo-electro-catalyst designed for the degradation of DOX in wastewater is obtained. Specifically, we present the use of blue TiO_2 nanotubes (BT) doped with cobalt ions as a novel electrocatalyst. By showcasing the versatile capabilities of the photocatalyst, this research highlights its potential in addressing both bacterial and organic contamination in water sources.

7.1 MATHERIALS AND METHODS

7.1.1 Obtaining photocatalysts.

7.1.1.1 Electrochemically obtained TiO_2 nanostructures.

Blue titanium dioxide (BT) nanostructures were obtained by anodizing recycled aerospace titanium plates (considered waste products from the production line) at 40 V for 2 h in a two-electrode cell.

7.1.1.2 Cobalt doping of blue TiO_2 nanostructures

In order to highlight the most effective method of Cobalt (Co) doping of previously obtained BT on titanium, two methods were applied: electrochemical technique and plasma treatment.

For the Co electrochemical doping technique, the pulsed chronoamperometry method (BT/Co-E) was used and the Cobalt-TiO_2-blue plasma composite (BT/Co-P) was obtained by cobalt doping using the magnetron sputtering method in plasma on BT board support.

7.1.2 Characterization and applicability of catalysts

The morphological, optical, and electrochemical characteristics of the obtained catalysts were studied. Antibacterial activity. The effectiveness of the antibacterial properties of the materials was measured against two different harmful microbial strains.

7.2 RESULTS AND DISCUSSIONS

7.2.1 Characterization of the synthesized electrodes

7.2.1.1 Physico-chemical characterization of the obtained electrodes

Following metal doping, SEM images were recorded at different magnifications to examine different structures. The presence of electrochemically doped cobalt is evidenced by the formation of star-shaped nanostructures (BT/Co-E). Also, the EDX results for the BT/Co-P sample showed a small amount of cobalt of about 0.03%.

Contact angle analysis was used to investigate the wetting property of the samples. It can be seen from the results that BT/Co-E had a minimum contact angle. As the data show, the presence of Co was found to be more effective in reducing the contact angle.

Optical parameters - Bandgap energy and Urbach energy.

As reported in the literature, the broad band gap of TiO_2 limits its absorption to the ultraviolet rays of the solar spectrum, making titanium powders unsuitable for use as visible light absorbers. As a

result, the goal is to lower the band gap, which in this case is reduced from 3.04 eV for BT to 2.88 eV and 3.00 eV for cobalt-doped BT films by electrochemical and plasma methods, respectively.

Antibacterial activity

After carrying out the antibacterial activity tests, it is indicated that cobalt-doped blue TiO_2 nanostructures are very effective against Gram-negative and Gram-positive bacteria. One possible mechanism would be explained by the fact that when cobalt-doped TiO_2 is exposed to light, it can generate electron-hole pairs.

The antibacterial performance of cobalt-doped blue TiO_2 can vary depending on factors such as Co concentration, preparation method, light source, and exposure time. Optimizing these factors can maximize the antibacterial efficacy of nanostructures [16].

7.2.1.2 Electrochemical characteristics of the developed electrodes

Electrochemical impedance spectroscopy (EIS) and Mott Schottky (MS) were used to estimate the charge transfer and recombination process at the electrode/electrolyte interface. A Randles equivalent circuit was proposed to understand the electrode behavior by associating the arc radius with the charge transfer resistance (Rct) at the catalyst/NaCl solution interface obtained, which is in parallel with a constant, phase element (CPE). The Rct values for BT, BT/Co-E, and BT/Co-P were determined as 370 kΩ, 76 kΩ, and 143 kΩ, respectively.

7.2.2 Applicability of the BT/Co-E catalyst

Influence of pH on the photocatalytic degradation of DOX.

An aqueous solution of Doxycycline (DOX) undergoes photocatalytic oxidation, taking place at different pH values: 2.5, 6.5 and 9.5 respectively. In the presence of the BT/Co-E catalyst, the DOX solution presented a spectrum with two maxima, observed at 271 nm and 375 nm [215]. Better results on exposure of the catalyst to light are observed at a pH of 6.5, so compared to the other degradations at other pHs, the absorbance is significantly reduced.

Photo-electro-catalytic application.

Since the best catalytic photodegradation results were obtained at a pH of 6.5 in all further tests, a 6 mol/L DOX solution with a pH of 6.5 will be used. Both photodegradation and photoelectrodegradation tests were performed to create a dual system where DOX degradation from water occurs.

The efficiency of photodegradation and photoelectrodegradation will be compared here. DOX solution was photoelectrocatalytically degraded at three distinct potentials: 0.35 V, 0.50 V, and 0.80 V, to demonstrate the impact of potential on DOX degradation efficiency.

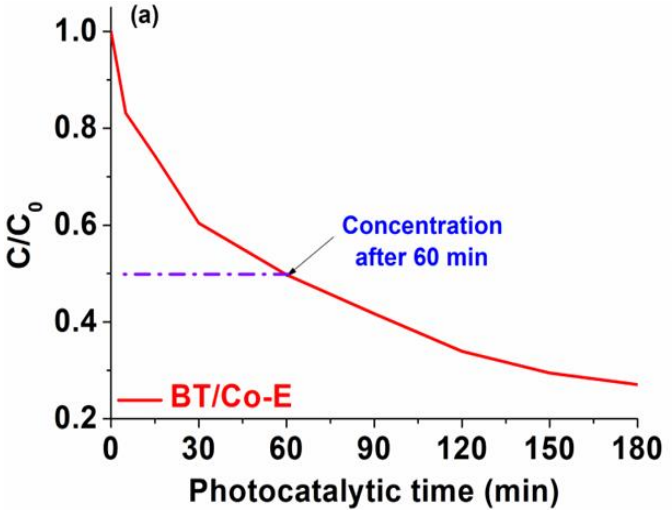

Fig. 7.11 a) Photoelectrocatalytic degradation efficiency

BT/Co-E and BT/Co-P photoelectrocatalysts were successfully produced using pulsed electrochemical deposition and magnetron plasma sputtering, respectively.

The results showed that the star-shaped composite film obtained by the pulsed electrochemical technique (BT/Co-E) offers the best results compared to the composite film obtained by plasma magnetron sputtering (BT/Co-P), due to the highest interfacial charge transfer efficiencies, slowest recombination rates, and superior conductivity.

The obtained catalysts were also studied from an antimicrobial point of view. The results showed that the presence of cobalt in both samples obtained improves the antibacterial activity against two bacteria.

CHAPTER 8

OBTAINING A GREEN, STABLE AND EFFICIENT PHOTOCATALYST BASED ON POLYDOPAMINE/TiO_2/CHLOROPHYLL

This study assumes the development of S-scheme mechanism-based models for TiO_2 heterostructures has made substantial contributions to improving the photocatalytic degradation of contaminants. In the present work, TiO_2 nanotubes (NTs) were obtained by anodizing on titanium surface. Then, the surface was modified with sustainable organic compounds by deposition of Polydopamine (PD) and/or Chlorophyll (Chl) to obtain a hybrid photocatalyst. The novelty of this study is highlighted by the presence of green and easy-to-obtain materials, PD and Chl used for the first time simultaneously and deposited on the surface of TiO_2 nanotubes to generate a double S-scheme photocatalyst. To test the stability and efficiency of the newly developed photocatalyst, methyl orange (MO) dye was selected as the sample organic compound. MO is widely used in printing, textile, food and pharmaceutical industries [10].

8.1 MATERIALS AND METHODS

8.1.1 Solutions and photocatalyst preparation

Spirulina chlorophyll extraction. Chl extraction was done according to literature [11], with some modifications. In order to extract Chl, a specific weight of spirulina is mixed with ethanol, followed by heating 5 minutes the mixture at 65°C.After cooling the mixture, the solution was centrifuged 20 min at 3000 rpm and 20°C.

Development of TiO_2 nanotubes-based photocatalysts doped with chlorophyll and polydopamine. TiO_2 nanotubes (**NT**) were obtained at 30V for 3h via anodization process of titanium plate in a two-electrode cell where carbon-graphite was used as counter electrode. The precursor electrolyte contains 0.01M ammonium fluoride (NH_4F), 2% (vol.) of water and ethylene glycol (EG). Anodized TiO_2 films were ultrasonicated in distilled water to remove the nanograss layer and calcined at 450°C for 1h [12]. Then, the deposition of Chl and PD was performed to improve photocatalytic activity.

Therefore, **NT/Chl** photocatalyst was created by immersing the NT plate in a concentrated previously obtained Chl solution for 1 hour, in dark conditions, then dried at room temperature. **NT/PD** electrodes were also obtained by immersing the NT substrate, for 1 hour, in a solution based on 1.3 x 10^{-5} mol/L dopamine (DA) (Sigma Aldrich) and 10 mL Tris buffer obtained from Trizma® Base (and HCl (Sigma Aldrich), with pH 8.5[13]. The samples were then washed well with pure water and dried. **NT/PD-Chl** photocatalyst was obtained as follows: the NT plate was immersed in a 9:1 mixture of DA and Chl and kept for 1 hour in the dark under stirring:

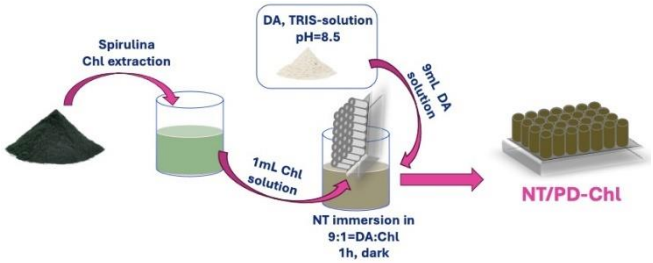

Fig. 8.1 A schematic figure showing the obtaining steps of newly photoelectrocatalyst: NT/PD-Chl

8.1.2 Equipments and substances used

In this subchapter, all the equipment, substances and techniques used for the development of this study were presented.

8.2 RESULTS AND DISCUSSIONS

8.2.1 Characterization of Chl extract and PD solution

The ethanol extracted Chl from spirulina has a green color and maximum absorbance peaks at 665 nm (Q spectral region, Qy band) in the red part of the spectrum and at 426 nm and 417 nm (Bands B_x and B_y in the Soret spectrum) in the blue domain (Figure 2c). This shows that Chl-a is much more abundant than Chl-b. This agrees with prior studies that found the Chl-a to be the dominant form of Chl during ethanol extraction of spirulina, as is the case of most photosynthetic oxygenated organisms[14]. The Soret and Q spectral bands arise from the $\pi \rightarrow \pi^*$ transitions of the four boundary orbitals [15] being polarized along the x-axis (B_x, Q_x) and y-axis (B_y, Q_y), respectively, axes that pass through the N atoms[16] in the porphyrin ring. The porphyrin ring structure of Chl-a, with a network of delocalized bonds and orbitals (as shown in Fig. 2a), allows it to absorb only the energy of high-intensity visible photons in sunlight and thus can be used as an efficient photoreceptor. This finding highlights the importance of Chl-a as an antenna for capturing light essential for photosynthesis [17].

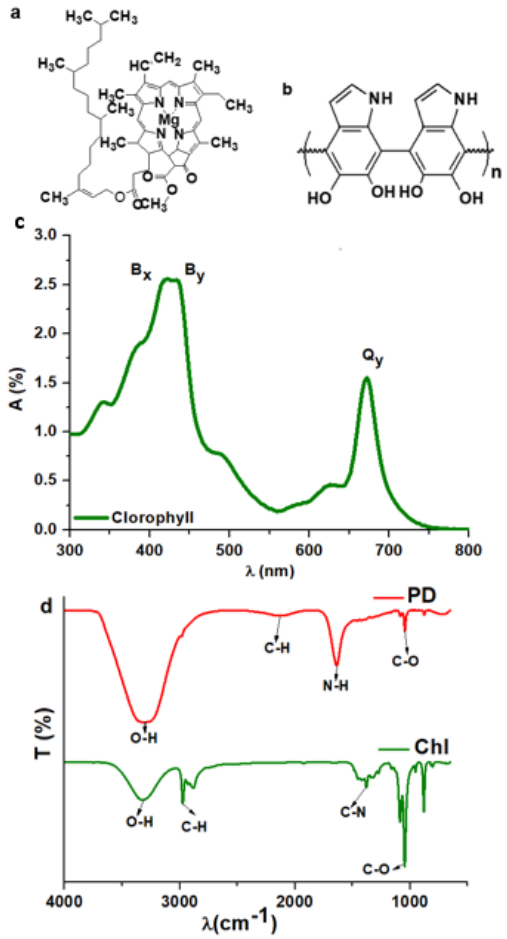

Fig. 8.3 Molecular structure (a) Chl and (b) PD. Absorption spectra at room temperature of (c) Chl extract and respectively (d) FTIR spectra for Chl extract and PD solution.

The Chl-a concentration extracted from spirulina is 17.872 mg/cm^3, and was estimated using the method developed by R.J. Ritchie [18], valid when the solvent is ethanol.

8.2.2 Photocatalysts characterization

8.2.2.1 Photocatalysts surface characterization

SEM analysis shows the morphology of the electrochemically grown TiO_2 layer on titanium surface for NT sample, Fig. 8.4 a). Observing the micrographs taken at low magnification, the oxide layer is visible on the entire surface taking over the morphology of the titanium substrate. In high magnification micrographs, the nanotube structures with a uniform distribution on the surface are visible. The diameters of the nanotubes are between 45 and 80 nm. Tubes with larger diameter have a low total surface area which have a detrimental impact on photocatalytic activity, but increase the light transmission, which improves the photocatalytic activity [19]. We believe that the diameter of the nanotubes developed in this study achieves a balance between these two effects tendency on photocatalytic activity. The SEM micrographs for NT/Chl reveal successful Chl deposition, making the nanotubes slightly less visible (Fig. 8.4 d, e.). The overlapping EDS mapping of Mg and N components shows homogeneous Chl distribution on nanotube surfaces (Figure 8.4f)). For NTs/PD sample, the uniform PD deposition keeps nanotube open without a significant influence on the tube diameter. (Fig. 8.4 g-i)). PD-Chl deposition changes morphology for NTs/PD-Chl. Low-magnification micrographs show groove-like structures (Figure 8.4j)). Figure 8.4k) shows a porous film with a spider web-like fibrillar structure with three-dimensional arrangement obscuring TiO_2 NT.

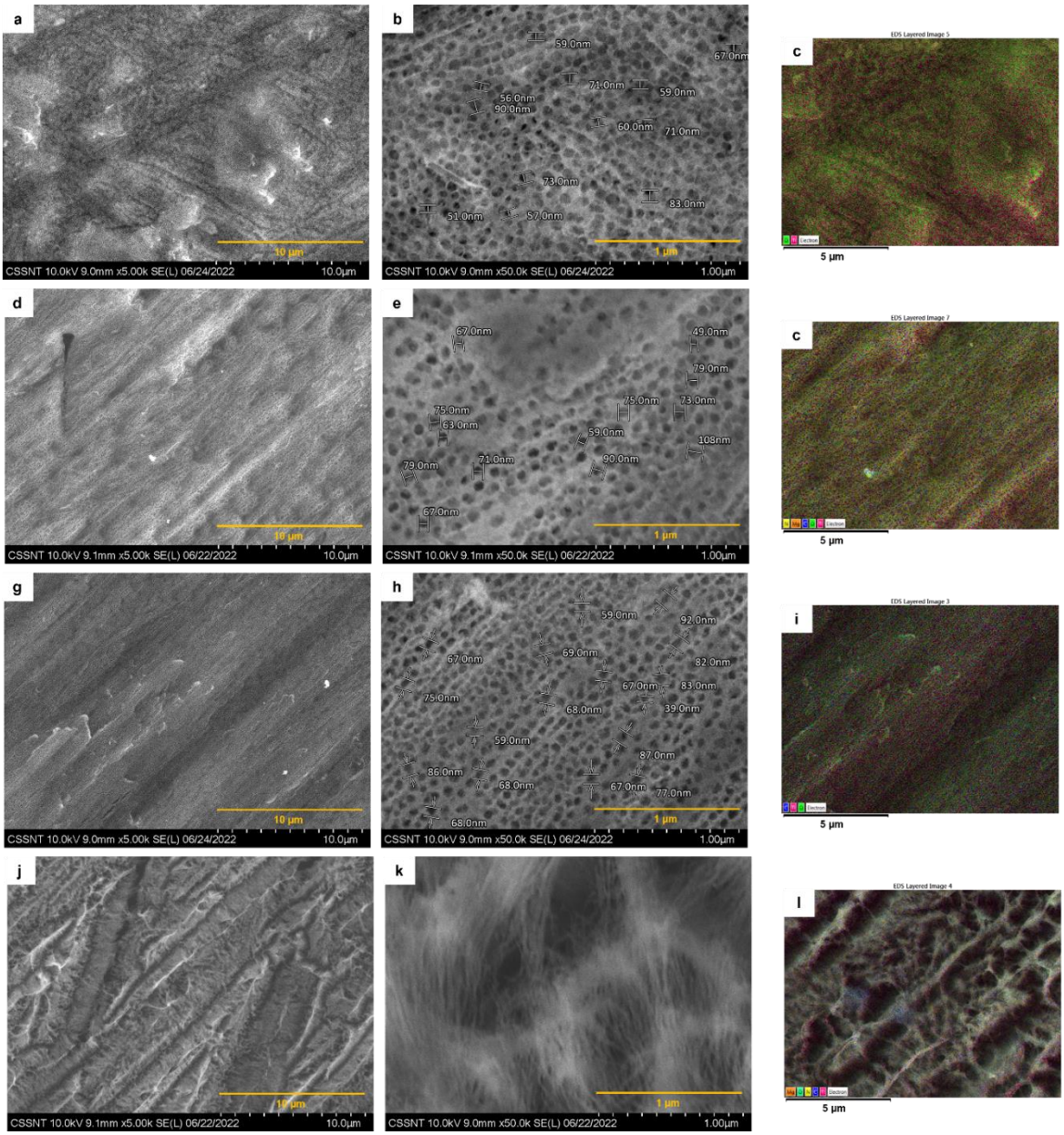

Fig. 8.4 SEM images and EDX analysis for NT (a, b, c) NT/Chl (d, e, f) NT/PD (g, h, i) and NT/PD-Chl (j, k, l).

AFM analysis reveals the surface roughness of NT, 359 nm, then Chl deposition smooths the surface to 85 nm for NT/Chl. NT/PD and NT/PD-Chl have quasi-similar roughness values of 141 and 146 nm, respectively.

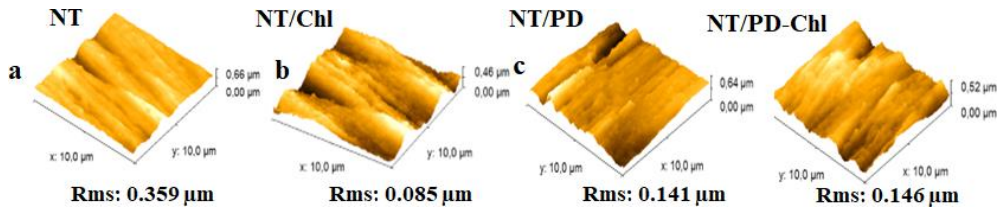

Fig. 8.5 AFM image showing the roughness of the obtained surfaces

FT-IR spectroscopy was used to evaluate the interactions between the TiO_2 nanostructured surface and coatings, Fig. 8.6.

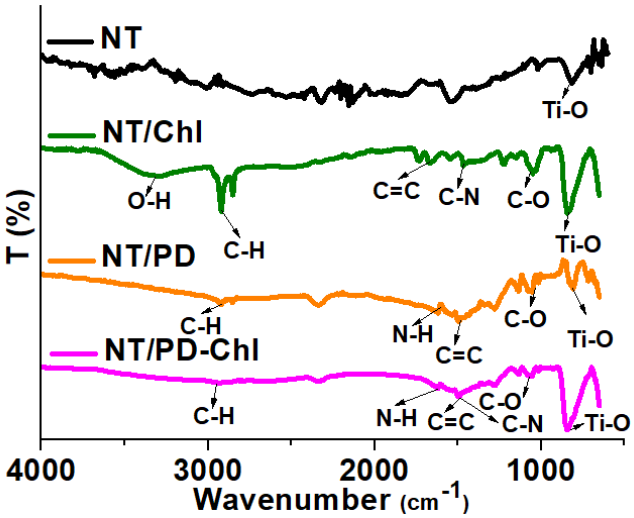

Figure 8.6. The obtained photocatalysts' FTIR (Fourier Transform Infrared) spectra.

X-Ray diffraction analysis. The phase purity and crystallinity of NT uncoated and coated surfaces were examined by X-Ray diffraction analysis (XRD). The following features were used to distinguish the TiO_2 anatase phase in all samples: space group I 41/a m d:1(141/0) and cell parameters (Alpha = 90.000, Beta = 90.000, Gamma = 90.000, Volume = 136.933, Z = 1).

Chl and PD were not directly identified by XRD analysis, but their presence could be sustained by the slight shifts in the positions of the peaks in the samples containing them.

Micro-Raman Spectroscopy. Anatase TiO_2's four typical Raman active modes, with symmetries E_g, B_{1g}, A_{1g} and E_g and 618 cm^{-1}, are clearly visible in all samples.

In the Raman spectra of NT/PD, two new peaks appeared at at 1370 cm^{-1} and 1570 cm^{-1} because of PD. The new peaks arise from catechol, a crucial building block of the DA structure, being stretched (1370 cm^{-1}) and deformed (1570 cm^{-1})[20]. These peaks are also visible in sample NT/PD-Chl. NT/Chl shows many Raman signals in the range of 950 cm^{-1}–1800 cm^{-1} for Chl-a. The main identified peaks are 980 cm^{-1}, 1070 cm^{-1}, 1115 cm^{-1}, 1147 cm^{-1}, 1205 cm^{-1}, 1308 cm^{-1}, 1455 cm^{-1} and 1555 cm^{-1}. A fraction of these bands is also present in sample NT/PD-Chl [21].

Wettability and surface energy. The samples wettability was examined, and NT hydrophilicity (15º) was attributable to its surface high polarity due to hydroxyl groups found in FTIR spectra and oxygen vacancy (OV) defects observed in XPS analysis. However, NT/Chl is very hydrophobic (119º) because Chl possesses a long hydrophobic chain (phytol chain) attached to one of its rings [22]. It has been found that the presence of hydrophobic Chl-a dye molecules on surfaces could reduce the interaction between aqueous electrolyte and catalyst surface [23]. Aside from this, PD presence on NT surface decrease the –OH groups density[24] and leads to an insignificant increase in contact angle value (52º). Contact angle found in NT/PD-Chl is around 69º which sustains the presence of PD and Chl on the NT surface. Since Chl is in low ratio in PD-Chl mixture (9:1 = DA: Chl), the contact angle decreases comparing to NT/Chl and increases comparing to NT/PD sample.

Photocatalytic reactions depend on surface modification reflected on surface free energy (SE). The SE changes depend on the atomic level of coordinative unsaturation. Free energy at the surface of

the catalyst is affected by the amount of oxygen vacancies, the charge density and roughness. A greater surface energy typically denotes a more reactive surface but the sample can become thermodynamically unstable [25]. The SE can be used as a new, effective way to describe catalytic activity with a volcano-shaped correlation [26]. The best catalytic performance was obtained for medium values of SE.

In this study, SE has been explored effectively using the Owens-Wendt-Rabel-Kaelble (OWRK) model, Table 8.1.

Table 8.1 Contact angle values, surface energy, roughness measurements

Sample	Contact Angle (°)			SE (mJ/m^2)	Molecular attraction
	DI water	EG	DMSO		
NT	15±0.33	12 ±0.46	13 ±0.27	71	Strong
NT/Chl	119 ±0.53	100 ±0.82	108 ±0.75	7	Weak
NT/PD	52 ±1.09	18 ±0.66	11 ±0.18	49	Strong
NT/PD-Chl	69 ±0.65	43 ±0.29	42 ±1.46	36	Medium

X-ray photoelectron spectroscopy. The XPS analyses were used to investigate their surface elemental composition. Figure 6 displays the XPS survey spectra of modified TiO_2 films, which reveal the appearance of the peak of C and N due to Chl and PD deposition.

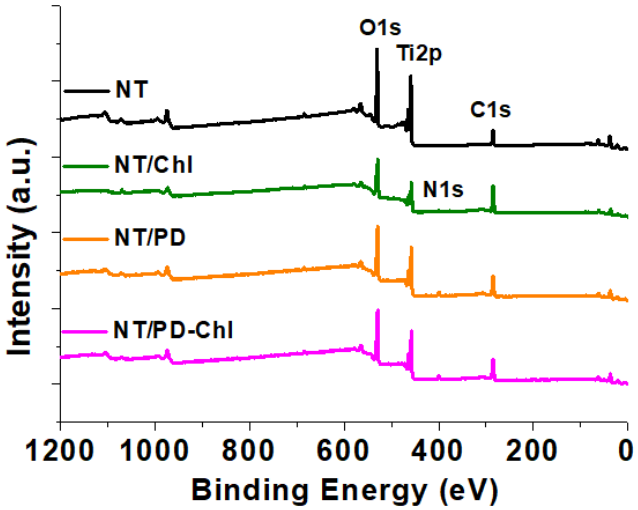

Fig. 8.9 XPS survey spectra of modified TiO_2 films.

Considering that XPS is a surface sensitive technique used to analyze the outermost (~10 nm) surface layer, for NT sample, the relatively high percentage of carbon could be attributed to traces of ethylene glycol left in the outer oxide layer after anodization. The presence of ethylene glycol on the surface makes it difficult to assess the Ti:O ratio, but it is obvious that it deviates from the 1:2 stoichiometric ratio suggesting Ti^{3+} defects and oxygen vacancies on the surface. For NT/Chl, the percentage of N is 1.76%, corresponding to 24.2% C according with the C:N ratio from Chl. This percent cumulated with the % C from NT uncoated sample is almost equal with the total carbon percentage from NT/Chl sample, 53.2%. This observation correlated with the decrease of Ti percentage could mean a deposition of a thin layer of Chl which covers a part of uncoated TiO_2. Due to preferential bonding on the ethylene glycol areas, PD deposition does not appreciably modify Ti percentage compared to

uncoated NT. For NT/PD-Chl, correlation between the obtained C and N percentage sustains the 9:1=PD:Chl ratio used for deposition. An important percentage of Ti is also found showing that a part of titanium oxide remains uncoated or partially coated being able to be involved in the photocatalytic process in a S-scheme configuration.

Table 8.2. The atomic composition percentage of samples based

SAMPLE	TI2P %	O1S %	C1S %	N1S %
NT	20.72	49.42	27.53	-
NT/Chl	8.58	33.17	53.32	1.76
NT/PD	17.18	48.3	26.71	5.17
NT/PD-Chl	12.47	39.34	40.29	4.92

Regarding the binding oxygen, TiO_2 exhibits a very high energy value ~530eV (1 s). In the O1s area, lattice oxygen and hydroxyls are formed so there are three energies found at 530.6 eV, 532.1 eV, and 533.5 eV. All three energies match to oxygen bonding such as O-Ti found to be at the highest peak 530.6eV, O-H found to be at 532.1eV and oxygen bonded to carbon O-C for the peak at 533.5 eV. Signals from the oxygen lattice, including hydroxyls and water molecules, are already abundant in the 530-534 eV range. Ti^{3+} signal is associated with the oxygen vacancies formation at the surface and it has critical significance for the oxygen ions transfer within the lattices [27]. When the local electrostatic balance is disturbed and Ti^{4+} ion is converted to a Ti^{3+} ion, charge correction necessitates the introduction of an OV. Therefore, the OV states created by the Ti^{3+} species between the VBs and CBs are responsible for visible light response [28].

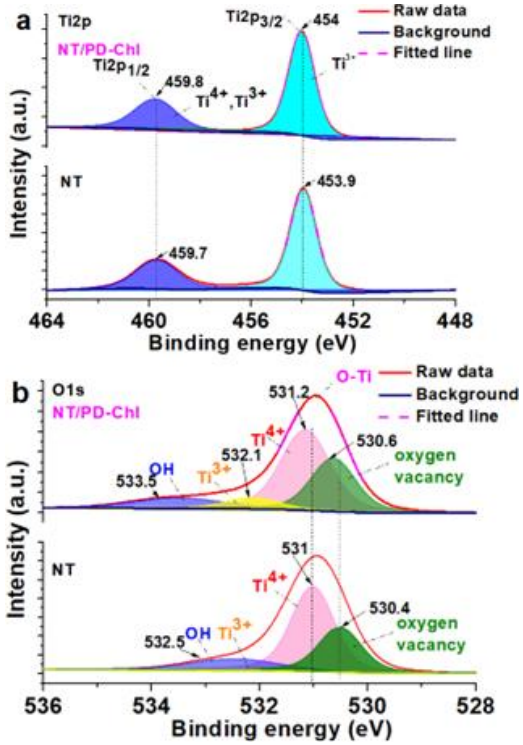

Fig. 8.10 (a)Ti2p and (b) O1s XPS spectra at high resolution

The XPS analysis indicated that the synthesized TiO_2 NT is more likely to include Ti^{3+} ions. Thus, bandgap narrowing in the modified TiO_2 NTs synthesized in aqueous ethylene glycol solution may be attributed to the existence of Ti^{3+} species.

UV-Vis analysis and Bandgap Energy

It is well known that TiO_2 anatase bandgap is wide, about 3.2 eV, however it has been shown that the bandgap of low-dimensional TiO_2 nanostructures obtained in our study is reduced (3.10 eV) giving more efficiency in light intake[29]. The equivalent band gap values of NT/Chl, NT/PD, NT/PD-Chl were calculated to be 3.08 eV, 2.98 eV and 2.90 eV respectively, based on the Tauc plot (Fig. 8.11) [30].

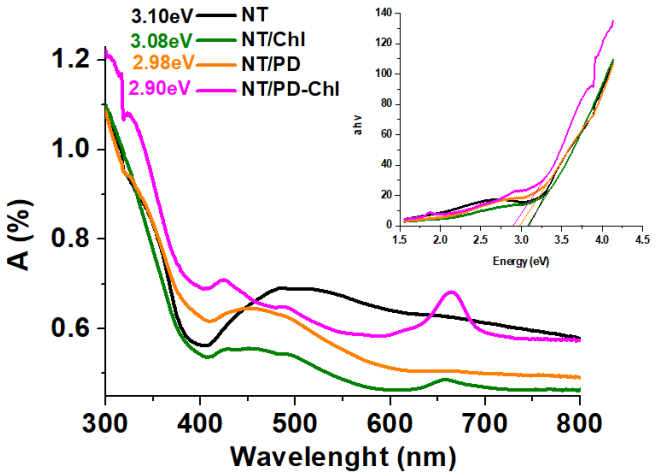

Fig 8.11 Absorbance spectrum recorded for all samples. Inset: band gap energy found from Tauc's Plot.

8.2.2.2 Photocatalyst electrochemical characterization

Cyclic voltammetry

Electrochemical interfaces of catalytic surfaces in contact with the MO electrolyte were characterized through cyclic voltammetry. The surface interactions at the oxide-solution interface influences the surface charge and determines the electrical double layer capacitance (C_{dl}) [31]. The surface charge dependent C_{dl} could be an essential structural feature for surface interactions with MO. Fig. 8.12 shows the CV curves for NT and modified surfaces during anodically polarization from -0.6V up to 1V vs. Ag/AgCl/0.1M KCl. The shape of the voltammograms shows a marginal capacitive current in the anodic region at over 0.5 V. C_{dl} was determined by dividing the average current density (I) measured over the potential sweep from 0.5 V to 1 V in the anodic direction by the scan rate (s), as shown in the CV plots [32]:

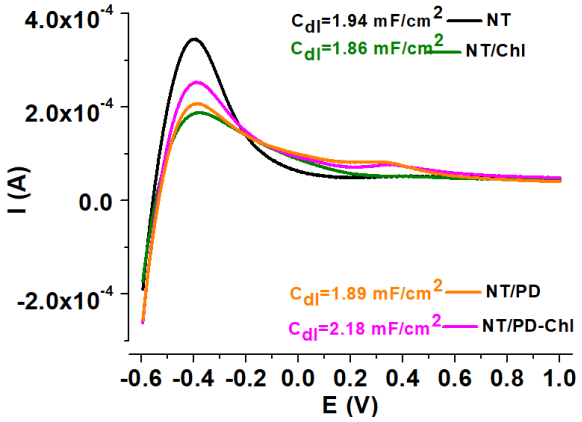

Fig. 8.12 The anodic branch of the cyclic voltammograms for NT, NT/Chl, NT/PD and NT/ PD-Chl, used for C_{dl} calculation.

For NT, the calculated value of C_{dl} is 1.94 mF/cm^2, close to other value presented in literature for self-doped TiO_2 NT (1.84 mF/cm^2)[33]. The deposition of Chl and PD onto nanotubes surface leads to a slightly decrease in C_{dl} (1.86 mF/cm^2 for NT/Chl and 1.89 mF/cm^2 for NT/PD, respectively) probably due to a possible barrier in double layer development on nanotubes in the presence of coatings[34]. However, as was revealed in SEM analysis, the nanotubes are not completely covered and the changes in the tubes diameters after deposition are not significant causing only a slight decrease in C_{dl}. On the other hand, for NT/PD-Chl, the deposition of three-dimensional porous film with a spiderweb fibrillar structure improves electric double layer development because of an increase in the active surface, 2.18 mF/cm^2.

Thus, the surface charge of TiO_2 was improved after surface modification with PD-Chl, changing the surface optical and electrical conductivity by creating new energy levels inside the bandgap.

Electrochemical impedance spectroscopy

To estimate the charge transfer rate and recombination, an EIS study was carried out at the electrode/MO solution interface. The obtained EIS results for NT and modified surfaces, NT/Chl, NT/PD and NT/ PD-Chl are presented in Fig. 8.13. A simple Randles equivalent circuit was proposed to describe the electrode behavior associating the arc radius with the charge transfer resistance (R_{ct}) across the electrode/electrolyte interface. The smallest R_{ct} value indicating the most efficient interfacial charge transfer and slowest recombination rate was obtained for NT/PD-Chl, 58 kΩ. The surfaces modified with PD and Chl showed larger R_{ct} values, 295 kΩ for NT/Chl and 401 kΩ for NT/PD, respectively. The highest value was obtained for unmodified NT sample, 496 kΩ, indicating poor charge transfer characteristics.

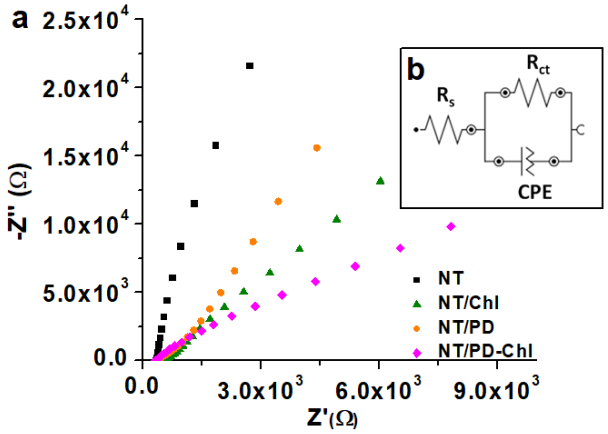

Fig 8.13 a) Nyquist plots for NT, NT/Chl, NT/PD and NT/ PD-Chl. b) proposed equivalent circuit

Mott-Schottky analysis

The E_{fb}, which depends on the recombination process and interfacial charge transfer [32], may be determined by extrapolating to $1/C_2 = 0$, from the Mott-Schottky plots. As would be expected for TiO_2, an *n*-type semiconductor, every studied sample had a positive slope on the Mott-Schottky graphs.

The calculated value of E_{fb} for NT is 0.38 V. Chl and PD deposition shifts the flat band potential position to more negative potentials, 0.18 V and 0.06 V. The largest shifting of the flat band potential was observed for hybrid NT/PD-Chl coating, 0.02 V. Thus, NT modified surface enhances the photo-catalytic abilities of the surface, especially for PD-Chl (NT/PD-Chl) photocatalysts showing that the surface state distribution has changed by bonding adlayers to the surface.

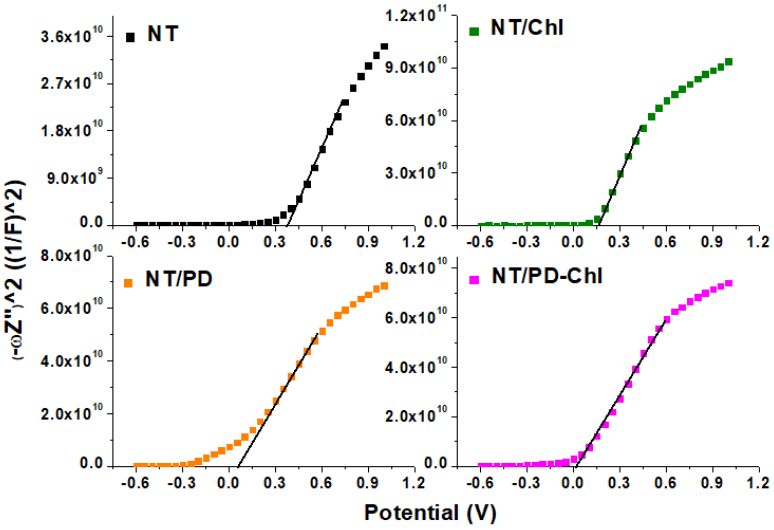

Fig. 8.14 Mott Schotky plots for NT, NT/Chl, NT/PD and NT/ PD-Chl

Band energy levels

The locations of all modified TiO_2 NTs' conduction bands (CBs) are addressed further. We have determined the positions of the conduction bands for all samples relating to the flat band values provided by the Mott-Schottky analysis. The edge of the conduction band is less than 0.1 V from its potential of the flat band [35], thus the CB levels were calculated at 0.28 eV for NT, 0.08 eV for NT/Chl, -0.04 eV for NT/PD, and -0.08 eV for NT/PD-Chl, respectively. The valence band (VB) positions were estimated knowing the CB positions and band gap energy values. NT_{VB} was located around 3.38 eV. When the NT surface was modified, a shift was observed in the VB and CB locations. Compared to NT, the VB

position of NT/Chl, NT/PD, and NT/PD-Chl were shifted to 3.16 eV, 2.94 eV, 2.82 eV, respectively. A contrast graphic of the four photocatalysts is displayed in the diagram below.

8.2.3 Photocatalytic degradation of Methylorange

Photoelectrochemical behavior

Photoelectrochemical behavior. The photocurrent response was evaluated by chronoamperometry measurements in MO aqueous solution at a bias of 0.35 V vs. Ag/AgCl, by on-off cycles registered under illumination-dark. In the first 5 minutes of the first dark-light irradiation cycle the highest current value was recorded for the NT catalyst, about 60 $\mu A/cm^2$, but starting with the second cycle, the current drastically drops reaching a lower value of about 15 $\mu A/cm^2$ after 25 minutes. This photo-electro-catalytic behaviour indicates that the NT surface is very active at the beginning of light irradiation, probably due to the more hydrophilic surface, higher surface energy (71 mJ/m^2) and a strong interaction with MO. However, its photostability is low and electron-hole recombination proceeds rapidly, therefore decreasing its photocatalytic properties. The XPS and EIS results confirm these observations demonstrating that the NT/MO MO degradation solution interface exhibited poor charge transfer properties.

In the case of the NT/Chl catalyst, the photocurrent of the first dark-light irradiation cycle is lower compared with NT probably due to the weak molecular interaction between MO and NT/Chl hydrophobic surface with a lower surface energy (7 mJ/m^2). Then the photocurrent slowly decreases from 35 $\mu A/cm^2$ to the quasi-constant value of 22 $\mu A/cm^2$ reached after about 10 minutes and it fails to stabilize even after 180 minutes. Moreover, starting with the third cycle, the photocurrent response is higher than the one corresponding to the NT sample suggesting that the process of electron-hole recombination is slowing in the case of NT/Chl, likely as a result of electron transfer from Chl HOMO level to TiO_2CB under photoirradiation [36, 37]. Also, the corresponding NT/Chl charge transfer resistance is lower than that of the NT catalyst according to EIS measurements, demonstrating a higher charge transfer efficiency for NT/Chl. Nevertheless, the stability is better than that of NT, but the current still decreases over time. This could be due to the desorption of sensitizer from TiO_2 surface as was already suggested [38] or to the photodegradation and a lower stability of Chl in interaction with the nanostructured NT surface. Although, the Chl-a solution stability in the natural environment was demonstrated, it seems that the interaction between the hydrophobic Chl coating and hydrophilic NT surface is weak resulting in photocatalyst instability and poor performance in time.

For NT/PD-Chl, a synergy between the features of PD and Chl occurred. The photocurrent response for NT/PD-Chl was higher than that of NT/PD and NT/Chl, which indicates that the presence of Chl and PD sped up the catalytic activity at the beginning of the light irradiation. Otherwise, the presence of PD-Chl thin layer on the NT surface (according to SEM image, Figure 3j, k.) increases the stability of the photocurrent response over time. After the second dark-light irradiation cycle, the photocurrent values increased slightly as the electron-hole combination process was probably suppressed because of the photogenerated electron transfer from Chl to NT and from PD to NT (according to photodegradation mechanism, see Figure 13) under light irradiation and lowest charge transfer resistance as was revealed by EIS data.

The chronoamperometry plots sustained by EIS and MS measurements demonstrate that loading TiO_2 NT with Chl and PD enhances electron transport and the rate of electron-hole recombination at the interfacial heterojunction resulting the highest and most constant photocurrent response.

MO photocatalytic degradation.

MO aqueous solution was used to study the photocatalytic activity and all tests were carried out three times. Under light conditions (Figure 8.17.a)) it can be observed that there was almost no photolysis of MO, in the absence of catalysts, in the first 180 minutes. MO degradation efficiency reached 68.4, 93.55, 90.15, and 97.74% when NT, NT/Chl, NT/PD, and NT/PD-Chl were exposed to visible light for 180 minutes.

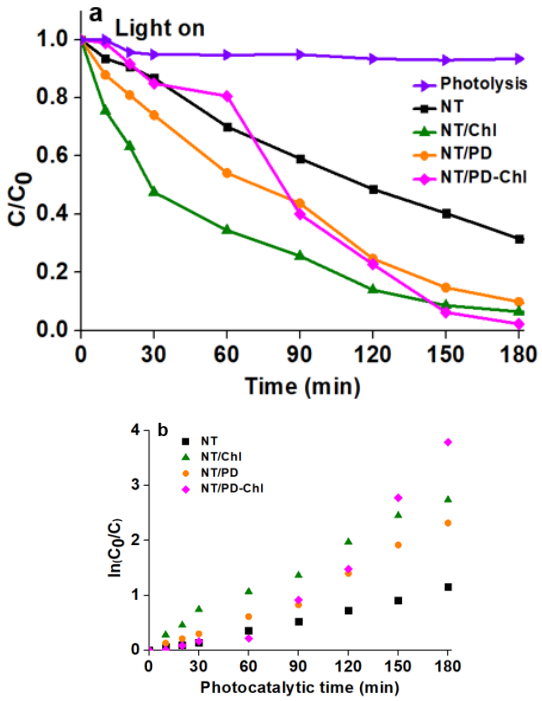

Fig. 8.17 (a) MO photodegradation efficiency; (b) Reaction kinetics

(Initial conditions: 2.5×10^{-5} mg L^{-1}MO, 25 °C).

Fig. 8.17, which illustrates the photodegradation curve of the MO solution, shows two degradation efficiency tendencies for all samples over the period of 180 minutes. Thus, considering the obtained values after light exposure, two degradation kinetics were performed.

ROS generation

To explore ROS formation, the ESR spectra were acquired after 20 minutes of UV-Vis lamp irradiation of each sample.

FINAL CONCLUSIONS

This work aims to use electrochemical methods to produce the oxidation of organic pollutants found in water. Modified titanium dioxide substrates were obtained to successfully produce the photocatalysis and photoelectrocatalysis processes to produce the degradation of organic pollutants.

Thus, TiO_2 thin films formed by dip coating on an FTO substrate were successfully obtained and characterized using surface, optical and electrochemical techniques. The impact of the dispersant (polyethylene glycol-PEG) on the surface (morphology, wettability, surface energy), optical (band gap and Urbach energy) and electrochemical (resistance to charge transfer, flat band potential) properties was investigated. When PEG was added to the sol-gel solution, the optical gap energy of the resulting films was reduced from 3.25 to 3.12 eV, and the Urbach energy increased from 646 to 709 meV. The addition of dispersant in the sol-gel process influences the surface characteristics, as evidenced by lower contact angle values and a higher surface energy obtained. Electrochemical measurements (cyclic voltammetry, electrochemical impedance spectroscopy, and Mott-Schottky analysis) revealed improved catalytic properties of the TiO_2 film, due to a higher rate of proton insertion into the nanostructured TiO_2, as well as a decrease in the charge transfer resistance from 418 k to 23.4 k and a drop in the flat band potential from 0.055 eV to -0.019 eV. The obtained TiO_2 films represent a promising alternative for technological applications due to their advantageous surface, optical and electrochemical characteristics, these characteristics being evidenced by the photodegradation efficiency of MO up to 56%.

TiO_2 nanotubes obtained by anodic oxidation on which TiO_2 nanofibers were deposited by electrospinning were also successfully obtained. The obtained data confirm the influence of the surface properties on the optical and photocatalytic character. Thus, the bandgap energy decreased considerably from 3.20eV to 3.05eV, which is obviously due to the deposition method of TiO_2 nanofibers on the previously anodized TiO_2 surface. The SEM images also confirm that a larger contact surface is obtained making the photocatalysis process more efficient. The proposed application was the degradation of an aqueous solution of tetracycline and the data shows a degradation yield of 80%.

Another study compares two simple doping methods by electrochemical deposition and plasma deposition for the production of cobalt blue-TiO_2-cobalt (Co) catalyst films with improved catalytic and antimicrobial properties. The obtained catalysts were subjected to electrochemical tests, optical analysis and also characterized in terms of morphology, wettability and antibacterial effect to understand and analyze the impact of the cobalt doping method on the final catalyst characteristics. The composite film formed by the electrodeposition of Co on the blue-TiO_2 nanostructures is characterized by a higher amount of Co doped, which leads to a more hydrophilic behavior, a maximum charge transfer efficiency at the interface, a lower recombination rate and better p-type conductivity and improved antibacterial activity. Also, by using this electrochemical doping technique, the Urbach energy was increased from 1.171 to 3.836 eV, while the bandgap energy was decreased from 3.04 to 2.88 eV, due to the increase in the number of states of defects located in the band gap of TiO_2. For the bacterial tests, both gram-positive and gram-negative bacteria were used. In addition, photodegradation and photoelectrodegradation experiments using an aqueous doxycycline (DOX) solution were performed to determine the practical relevance of the research results. The synergistic combination of light and applied potential leads to 70% DOX degradation after 60 minutes of irradiation of the newly obtained photocatalyst.

In the latest study that was inspired by natural photosynthesis, a new green catalyst with better photocatalytic properties was obtained. Nanostructured TiO_2, chlorophyll-a (Chl) as an electron promoter, and a mussel-derived polydopamine (PD) bioadhesive were synergistically combined to

obtain a hybrid photocatalyst. The role of PD as a bridging molecule between Chl pigments and TiO_2 was clearly demonstrated by the enhanced charge transfer and recombination rate. To test the stability and efficiency of the new photocatalyst, an aqueous solution of methylorange was synthesized and used in subsequent photocatalysis tests. This challenging approach to obtaining new bio-inspired catalysts is in line with the new vision of obtaining photocatalysts.

The results of this study show the efficacy and stability of the new photocatalyst. Based on the combined effect of PD functionalization and Chl sensitization, the newly developed photocatalyst had the best photoelectrocatalytic performance for the degradation of methylorange, which was found to be 97.74% after 180 min. The data of this study were original and disseminated in a specialist article.

FUTURE RESEARCH DIRECTIONS

As future perspectives we propose:

- Testing the efficiency of these photocatalytic materials obtained on a pilot plant that simulates the natural environment.
- Aims to test a wider range of emerging contaminants such as various cosmetics or pharmaceuticals.
- Following the photocatalysis and electrophotocatalysis processes, we aim to develop HPLC and TOC methods to accurately observe the degradation compounds resulting from the process.
- Proposing some appropriate degradation mechanisms for these photodegradation processes.
- It also aims to develop a dual-function photoelectrochemical (PEC) system at laboratory scale, which simultaneously contributes to the degradation of organic pollutants in wastewater and to the production of hydrogen.

BIBLIOGRAPHY

1. Mandal S, Kunhikrishnan A, Bolan N, Wijesekara H, Naidu R. Application of biochar produced from biowaste materials for environmental protection and sustainable agriculture production. Environmental Materials and Waste: Elsevier; 2016. p. 73-89.
2. Gwenzi W, Simbanegavi TT, Marumure J, Makuvara Z. Ecological health risks of emerging organic contaminants. Emerging Contaminants in the Terrestrial-Aquatic-Atmosphere Continuum:. 2022:215-42.
3. Lombi E, Hamon R. Remediation of polluted soils. Encyclopedia of Soils in the Environment. 2005;4:379-85.
4. Tripathi A, Narayanan S. Impact of TiO2 and TiO2/g-C3N4 nanocomposite to treat industrial wastewater. Environmental nanotechnology, monitoring & management. 2018;10:280-91.
5. Zhao Y, Linghu X, Shu Y, Zhang J, Chen Z, Wu Y, et al. Classification and catalytic mechanisms of heterojunction photocatalysts and the application of titanium dioxide (TiO2)-based heterojunctions in environmental remediation. Journal of Environmental Chemical Engineering. 2022;10(3):108077.
6. Han F, Kambala VSR, Srinivasan M, Rajarathnam D, Naidu R. Tailored titanium dioxide photocatalysts for the degradation of organic dyes in wastewater treatment: a review. Applied Catalysis A: General. 2009;359(1-2):25-40.
7. Liu Y, Chen R, Zhu X, Ye D, Yang Y, Li J, et al. 3D radially-grown TiO2 nanotubes/Ti mesh photoanode for photocatalytic fuel cells towards simultaneous wastewater treatment and electricity generation. Journal of Cleaner Production. 2022;381:135200.
8. Dette C, Pérez-Osorio MA, Kley CS, Punke P, Patrick CE, Jacobson P, et al. TiO2 anatase with a bandgap in the visible region. Nano Lett. 2014;14(11):6533-8.
9. Natarajan S, Bajaj HC, Tayade RJ. Recent advances based on the synergetic effect of adsorption for removal of dyes from waste water using photocatalytic process. Journal of environmental sciences (China). 2018;65:201-22.
10. Hii HT. Adsorption isotherm and kinetic models for removal of methyl orange and remazol brilliant blue R by coconut shell activated carbon. Tropical Aquatic and Soil Pollution. 2021;1(1):1-10.
11. Martí-Quijal FJ, Ramon-Mascarell F, Pallarés N, Ferrer E, Berrada H, Phimolsiripol Y, et al. Extraction of Antioxidant Compounds and Pigments from Spirulina (Arthrospira platensis) Assisted by Pulsed Electric Fields and the Binary Mixture of Organic Solvents and Water. Applied Sciences. 2021;11(16):7629.
12. Fu F, Cha G, Denisov N, Chen Y, Zhang Y, Schmuki P. Water Annealing of TiO2 Nanotubes for Photocatalysis Revisited. ChemElectroChem. 2020;7(13):2792-6.
13. Tripathy J, Loget G, Altomare M, Schmuki P. Polydopamine-Coated TiO2 Nanotubes for Selective Photocatalytic Oxidation of Benzyl Alcohol to Benzaldehyde Under Visible Light. Journal of nanoscience and nanotechnology. 2016;16(5):5353-8.
14. Ritchie RJ. Consistent sets of spectrophotometric chlorophyll equations for acetone, methanol and ethanol solvents. Photosynthesis research. 2006;89(1):27-41.
15. Weiss CD, D. Electronic absorption spectra of chlorophylls. In The Porphyrins. Academic Press. 1978:pp. 211–23.
16. Kobayashi MA, M.; Kano, H.; Kise, H. . Spectroscopy and structure determination. In Chlorophylls and Bacteriochlorophylls. Springer. 2006;25.
17. Fiedor L, Kania A, Myśliwa-Kurdziel B, Orzeł Ł, Stochel G. Understanding chlorophylls: central magnesium ion and phytyl as structural determinants. Biochimica et biophysica acta. 2008;1777(12):1491-500.
18. Ritchie RJ. Universal chlorophyll equations for estimating chlorophylls a, b, c, and d and total chlorophylls in natural assemblages of photosynthetic organisms using acetone, methanol, or ethanol solvents. Photosynthetica. 2008;46(1):115-26.
19. Zhuang HF, Lin CJ, Lai YK, Sun L, Li J. Some critical structure factors of titanium oxide manotube array in its photocatalytic activity. Environmental science & technology. 2007;41(13):4735-40.

20. Challagulla S, Tarafder K, Ganesan R, Roy S. Structure sensitive photocatalytic reduction of nitroarenes over TiO2. Scientific Reports. 2017;7(1):8783.
21. Jiang L, Jin G, Kang J, Yu L, Yoon W, Lim M, et al. Surface characteristics of mussel-inspired polydopamine coating on titanium substrates. Journal of Wuhan University of Technology-Mater Sci Ed. 2014;29(1):197-200.
22. Queiroz MI, Fernandes AS, Deprá MC, Jacob-Lopes E, Zepka LQ. Introductory Chapter: Chlorophyll Molecules and Their Technological Relevance. Chlorophyll: IntechOpen; 2017.
23. Zidan G, Ann Greene C, Seyfoddin A. 2 - Formulation design in drug delivery. In: Seyfoddin A, Dezfooli SM, Greene CA, editors. Engineering Drug Delivery Systems: Woodhead Publishing; 2020. p. 17-41.
24. Negrescu AM, Mitran V, Draghicescu W, Popescu S, Pirvu C, Ionascu I, et al. TiO(2) Nanotubes Functionalized with Icariin for an Attenuated In Vitro Immune Response and Improved In Vivo Osseointegration. Journal of functional biomaterials. 2022;13(2).
25. Watanabe T, Yoshida N. Wettability control of a solid surface by utilizing photocatalysis. Chemical record (New York, NY). 2008;8(5):279-90.
26. Zhuang HL, Tkalych AJ, Carter EA. Surface Energy as a Descriptor of Catalytic Activity. J Phys Chem C. 2016;120(41):23698-706.
27. Idriss H. On the wrong assignment of the XPS O1s signal at 531–532 eV attributed to oxygen vacancies in photo-and electro-catalysts for water splitting and other materials applications. Surface Science. 2021;712:121894.
28. Xiong L-B, Li J-L, Yang B, Yu Y. Ti??+ in the Surface of Titanium Dioxide: Generation, Properties and Photocatalytic Application. Journal of Nanomaterials. 2012;2012.
29. Wang Z, Li J, Tang F, Lin J, Jin Z. Polydopamine nanotubes-templated synthesis of TiO 2 and its photocatalytic performance under visible light. RSC advances. 2017;7(38):23535-42.
30. Mîndroiu VM, Stoian AB, Irodia R, Trușcă R, Vasile E. Titanium Dioxide Thin Films Produced on FTO Substrate Using the Sol–Gel Process: The Effect of the Dispersant on Optical, Surface and Electrochemical Features. Materials. 2023;16(8):3147.
31. Zhang C, Huffer J, Sprik M. Coupling of Surface Chemistry and Electric Double Layer at TiO2 Electrochemical Interfaces. J Phys Chem Lett. 2019;10(14):3871-6.
32. Ungureanu C, Barbulescu L, Dumitriu C, Manole C, Pirvu C. Titanium industrial residues surface modification towards its reuse as antimicrobial surfaces. Environ Sci Pollut R. 2021;28(28):38224-37.
33. Zhou H, Zhang YR. Electrochemically Self-Doped TiO2 Nanotube Arrays for Supercapacitors. J Phys Chem C. 2014;118(11):5626-36.
34. Zhao XY, Wang YF, Zhu YX, Zhu L, Yang LB, Hou YD, et al. Frequency-dependence of electric double layer capacitance of TiO2-based composite nanotube arrays. J Electroanal Chem. 2016;779:199-206.
35. Kalanur SS. Structural, optical, band edge and enhanced photoelectrochemical water splitting properties of tin-doped WO3. Catalysts. 2019;9(5):456.
36. Bhardwaj S, Shekhawat MS, Suthar B, editors. Front Matter for Volume 1536. AIP Conference Proceedings; 2013: American Institute of Physics.
37. Phongamwong T, Barrabés N, Donphai W, Witoon T, Rupprechter G, Chareonpanich M. Chlorophyll-modified Au25(SR)18-functionalized TiO2 for photocatalytic degradation of rhodamine B. Applied Catalysis B: Environmental. 2023;325:122336.
38. Krishnan S, Shriwastav A. Chlorophyll sensitized and salicylic acid functionalized TiO2 nanoparticles as a stable and efficient catalyst for the photocatalytic degradation of ciprofloxacin with visible light. Environmental Research. 2023;216:114568.